Journal of Photochemistry and Photobiology A: Chemistry 316 (2016) 44–51

Contents lists available at ScienceDirect

Journal of Photochemistry and Photobiology A: Chemistry

journal homepage: www.elsevier.com/locate/jphotochem

Photophysics of an octasubstituted zinc(II) phthalocyanine incorporated into solid polymeric magnetic and non-magnetic PLGA–PVA nanoparticles

V.E. Diz[a,*], G. Leyva[b], R.D. Zysler[c], J. Awruch[d], L.E. Dicelio[e,*]

[a] INQUIMAE, Departamento de Química Inorgánica, Analítica y Química Física, Facultad de Ciencias Exactas y Naturales, Universidad de Buenos Aires, Ciudad Universitaria, Pabellón II, 1428 Buenos Aires, Argentina
[b] Instituto de Nanociencia y Nanotecnologia, Comisión Nacional de Energia Atómica, Avenida General Paz 1499, San Martín, 1650 Provincia de Buenos Aires, Argentina
[c] Centro Atomico Bariloche, 8400 Bariloche, Río Negro, Argentina
[d] Departamento de Química Orgánica, Facultad de Farmacia y Bioquímica, Universidad de Buenos Aires, Junín 956, 1113 Buenos Aires, Argentina
[e] INQUIMAE, Facultad de Ciencias Exactas y Naturales, Universidad de Buenos Aires, Ciudad Universitaria, Pabellón II, 1428 Buenos Aires, Argentina

ARTICLE INFO

Article history:
Received 3 July 2015
Received in revised form 31 August 2015
Accepted 19 October 2015
Available online 21 October 2015

Keywords:
Phthalocyanines
Solid nanoparticles
Poly(D,L lactide-co-glycolide)-polyvinyl alcohol
Magnetite
Singlet oxygen

ABSTRACT

2,3,9,10,16,17,23,24-octakis[(*N*,*N*-dimethylaminoethylsulfanyl)]phthalocyaninatozinc (II) (**S1**) was used as a lipophilic photosensitizer to be encapsulated into biodegradable poly(D,L lactide-co-glycolide)-polyvinyl alcohol nanoparticles. The synthesis, size, and spectroscopic, photophysical, and magnetic properties of nanoparticles, were analyzed. A greater number of sonication cycles afforded smaller nanoparticles. The stabilization by means of polyvinyl alcohol of all the nanoparticles synthesized provided a negative charge to the systems in a wide pH range. The thermograms obtained by differential scanning calorimetry showed that the nanoparticles were stabilized by polyvinyl alcohol. The incorporation of magnetite nanoparticles was verified by FT-IR, magnetization measurements by means of hysteresis curves and potential Z. S1 retained its efficiency in generating singlet oxygen. The incorporation of magnetite into the nanoparticles showed an increase in singlet oxygen quantum yields due to the heavy atom effect.

1. Introduction

Carriers are frequently used to deliver drugs through the body to protect them from degradation and excretion, to prevent adverse side effects of toxic drugs, or to accomplish targeted drug delivery. Different materials such as liposomes, micelles, gels, mesoporous silica nanoparticles, gold nanoparticles, and semiconductor quantum dots have been postulated as photosensitizer carriers [1–7].

Nanocarriers are used to improve the solubility, bioavailability and controlled release of drugs. However, there are some problems related to toxicity that require special attention [8]. Nanomaterials have special surface, size (0.1–100 nm), and macroscopic quantum tunneling effects. These properties allow nanoparticles to be used in fields such as medicine, electricity, optics, magnetics and catalysis [2,7,9–12].

Nanoparticles of biodegradable polymers can be used as injectable carriers for drug targeting [13]. Among them poly (D,L lactide-co-glycolide) (PLGA) nanoparticles have been used as drug carrier systems for many pharmaceutical drugs and photosensitizers [14,15]. However, the uptake of PLGA nanoparticles by the reticuloendothelial system after intravascular administration presents a major problem to procure an effective targeting to specific sites in the body. The strategy most commonly used to design long-circulating nanoparticles consists in coating them with hydrophilic or hydrophobic copolymers such as Polyethylene glycol (PEG) or polyvinyl alcohol (PVA) [16].

Magnetic nanomaterials are of particular interest and have been used in biological medicine, and also as drug carriers for biological molecular probes [17]. Superparamagnetic iron oxide nanoparticles covered with biocompatible polymers can yield powerful targeted delivery vehicles. These nanoparticles provide a stronger and more rapid magnetic response than bulk magnets when a magnetic field is applied. These nanoparticles can be routed to the target cell by applying a magnetic field [18,19].

* Corresponding authors. Fax: +54 11 4576 3341.
E-mail addresses: vdiz@qi.fcen.uba.ar (V.E. Diz), led@qi.fcen.uba.ar (L.E. Dicelio).

http://dx.doi.org/10.1016/j.jphotochem.2015.10.018
1010-6030/

On the basis of these results, further studies have been initiated to investigate the synthesis of magnetic nanoparticles encapsulated into biodegradable PLGA–PVA. In the present study, 2,3,9,10,16,17,23,24-octakis[(*N*,*N*-dimethylaminoethylsulfanyl)]-phtalocyaninatozinc(II) (S1) [20] was used as a lipophilic photosensitizer to be encapsulated into the nanoparticles. The spectroscopic, photophysical, photochemical, and magnetic properties, as well as the nanoparticle size, were analyzed.

2. Materials and methods

2.1. Materials

Poly(D,L lactide-co-glycolide) 50:50 (PLGA), polyvinyl alcohol (PVA, average Mw 9000–10,000 Da, 80% hydrolyzed), *N*,*N*-diethyl-4-nitrosoaniline 97%, imidazole ≥99%, tetrahydrofuran (THF) was of analytical grade, and methylene chloride (distilled) were purchased from Sigma-Aldrich. Methylene Blue (MB) was purchased from Fluka. Monodisperse magnetic nanocrystals stabilized with polyethyleneimine (PEI) was a gift from Centro Atómico Balseiro, Argentina [21]. 2,3,9,10,16,17,23,24-octakis[(*N*,*N*-dimethylaminoethylsulfanyl)]phthalocyaninatozinc(II) (S1) was synthesized as described elsewhere [22] (Fig. 1)

2.2. Instrumentation

Electronic absorption spectra were determined with a Shimadzu UV-3101 PC spectrophotometer and fluorescence spectra were monitored with a QuantaMaster Model QM-1 PTI spectrofluorometer. pH was measured with a Thermo pH meter Altronix TPX-1. Transmission electron microscopy (TEM) images were obtained by means of an EM 301 Phillips operating at 65 kV. Vortex-mixing was performed by means of a VELP Scientific ZX Classic. The sonicator used was MSE Soniprep 150. *Z* potential measurements were determined with a Zeta-Potential Analyzer (Brookhaven Instrument Corp.). Magnetic studies were carried out in a commercial superconducting quantum interferometer device (SQUID) magnetometer up to 10 kOe. Infrared spectra were recorded with a Perkin Elmer Spectrum One FT-IR spectrometer. Differential scanning calorimetry and thermal stability of the samples were performed with an SDT 2960 system (TA Instruments).

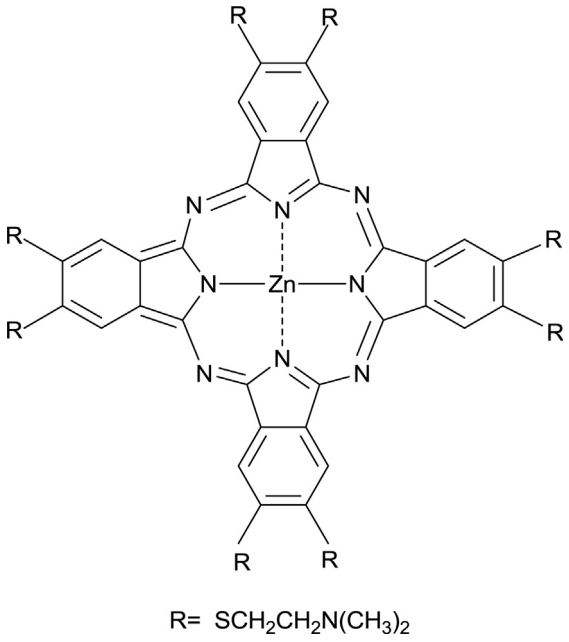

Fig. 1. Chemical structure of phthalocyanine S1.

2.3. Preparation of nanoparticles

Nanoparticles were prepared by an oil/water emulsion-solvent evaporation method [23]. PLGA was dissolved in methylene chloride at a final concentration in the range of 2×10^{-5} M–7×10^{-6} M. For blank nanoparticles (NPs), 10 mL of polymer solution was mixed with 20 mL of PVA 3% water solution and emulsified by one or more cycles for 10 min each in a 450 W ultrasonicator. The solution was then concentrated under reduced pressure with constant stirring, removing the organic solvent. Finally, the NPs obtained as a suspension were lyophilized and stored at 4 °C until further use.

Dye and magnetite were incorporated in the organic phase. The final concentration of the dye was 0.5 μM and 53 μM, whereas the magnetite concentration was 30 mg/mL solution.

2.4. Differential scanning calorimetry(DSC)

The composition of NPs was characterized by the analysis of the DSC curves. The curves were obtained in a DSC cell (Shimadzu DSC 60) using aluminium crucibles with about 3 mg of samples, under dynamic air atmosphere (100 mL/min) and heating rate of 30 °C/min at a temperature range from 20 to 500 °C. The DSC cell was calibrated with indium (m.p. 156.6 °C; ΔH_{fus} = 28.54 J/g) and zinc (m.p. 419.6 °C).

2.5. Z potential of blank nanoparticles (NPs) and nanoparticles with magnetite (NPs-Fe_3O_4)

The electrophoretic mobility of the particles was recorded from a total of 10 cycles of 50 seconds each according to Smoluchowsky's model with a residual error < 0.035 [24].

Measurements were performed at a concentration of 10^{-5} M for all nanoparticles. For all experiments, the ionic strength was kept constant by incorporating 0.15 M KNO_3 and adjusting the pH from 1.9 to 10.2.

2.6. Magnetic measurements

Magnetic measurements were performed at room temperature (T = 300 K) and T = 4 K for magnetite and at T = 5 K for NPs-Fe_3O_4 in the range of $H = \pm$ 10 kOe. The magnetization was normalized to the saturation value of the particles (about 40 emu/g in the systems studied).

2.7. Determination of S1 incorporation into NPs and NPs-Fe_3O_4

The incorporation efficiency was determined using UV–vis spectroscopy. The maximum absorbance intensity of S1 at 680 nm of the supernatant and washings after the incorporation of S1 into the NPs and NPs-Fe_3O_4 was subtracted from the starting concentration. The percentage of incorporation of S1 in all the nanoparticles was 33%.

Table 1
Monomer–dimer ratio and photophysical parameters of S1 in THF, S1–NPs and S1–NPs–Fe_3O_4.

	S1-THF[a]	S1-NPs	S1-NPs-Fe_3O_4
[S1]/M	1×10^{-7}	3.2×10^{-7}; 4.8×10^{-5}	3.2×10^{-7}; 4.8×10^{-5}
Monomer/Dimer	7.0	0.58; 0.46	0.60; 0.44
Φ_F	0.26	0.25; 0.11	0.03; 0.04
Φ_Δ	0.69	0.22; 0.11	0.23; 0.22

[a] Ref. [35].

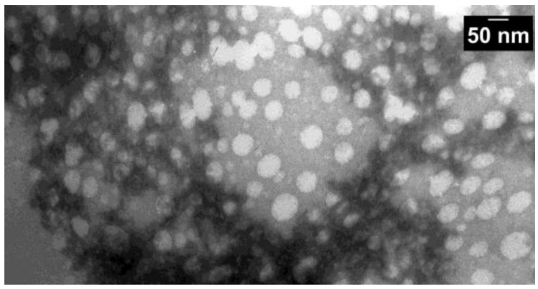

Fig. 2. Transmission electron microscopy following negative staining of NPs. Four sonication cycles.

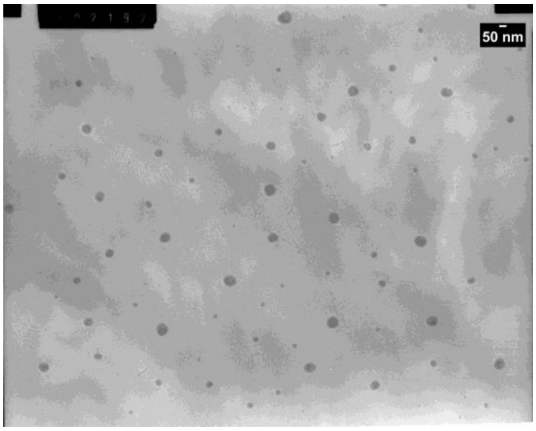

Fig. 3. Transmission electron microscopy following negative staining of NPs-Fe_3O_4. Four sonication cycles.

2.8. Photophysical properties

2.8.1. Spectroscopic studies

The absorption spectra of S1-NPs and S1-NPs-Fe_3O_4 were recorded at room temperature with a 300 μL 10 × 10 mm quartz cuvette.

The optical spectra and absorbed photon flow for scattering media were recorded on a Shimadzu UV-3101 PC spectrophotometer fitted with an integrating sphere. $BaSO_4$ was used as a white standard to adjust the 100% reflectance level. The absorbance spectra were recorded for samples with dyes (A_2) and for nanoparticles free of dyes (A_1) according to the geometry recommended by Lagorio [25,26]. The real absorbance spectra of the dyes were calculated according to Eq. (1) which represents the dye absorbance without taking into account the contribution of the support.

$$A = -\log\left(1 - \frac{10^{-A_1} - 10^{-A_2}}{2}\right) \quad (1)$$

2.8.2. Aggregation studies of S1 incorporated into the nanoparticles

An important aspect to consider is the strong tendency of phthalocyanines to form aggregates. As only monomers are capable to generate singlet oxygen, it is neccesary to evaluate the presence of aggregates. The strong tendency to aggregate is evidenced by the absoption spectra. The λ_{max} values and the shape of the spectra strongly depend on the solvent and dye concentration [27].

The intensity absorption ratio of the two bands corresponding to the monomer and oligomers was calculated. The higher values of the ratio indicated a disaggregated dye form [28]. This ratio was calculated for S1-NPs and S1-NPs-Fe_3O_4 by using the λ_{max} indicated in Table 1. These values were compared with those obtained in THF, where no aggregation was observed.

2.8.3. Emission spectra and fluorescence quantum yields

Fluorescence emission spectra of the scattering samples were obtained using a quartz cuvette of 1 mm optical path at a front face arrangement. Emission spectra were collected at an excitation wavelength of 685 nm (Q-band) (absorbances were under 0.1) and recorded between 700 and 800 nm. The emission spectrum of the reference for the fluorescence quantum yield calculation was also recorded between 700 and 800 nm exciting at 685 nm. Fluorescence quantum yields (Φ_F) of the doped samples were determined by comparison with S1 in THF as a reference ($\Phi_F = 0.26$) [21].

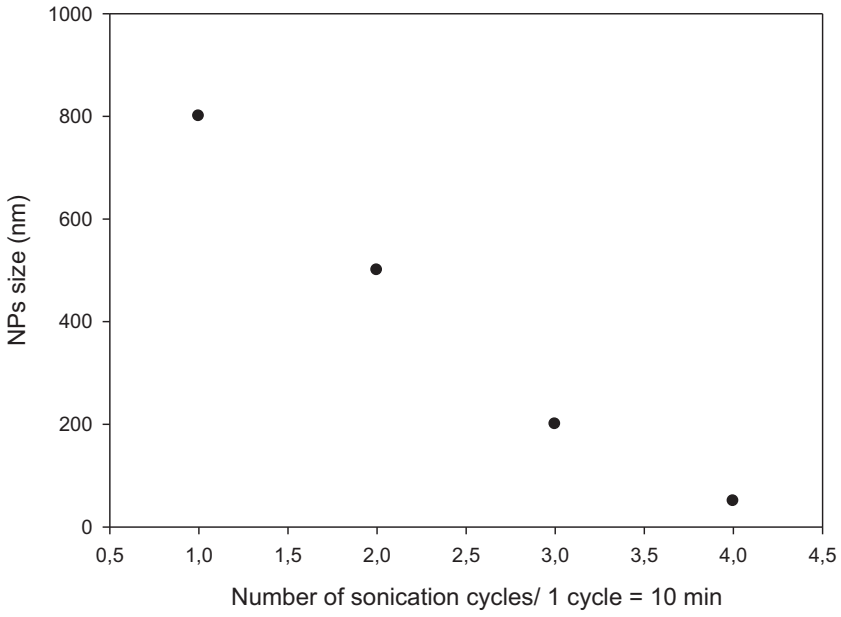

Fig. 4. NPs size versus number of ultrasonication cycles.

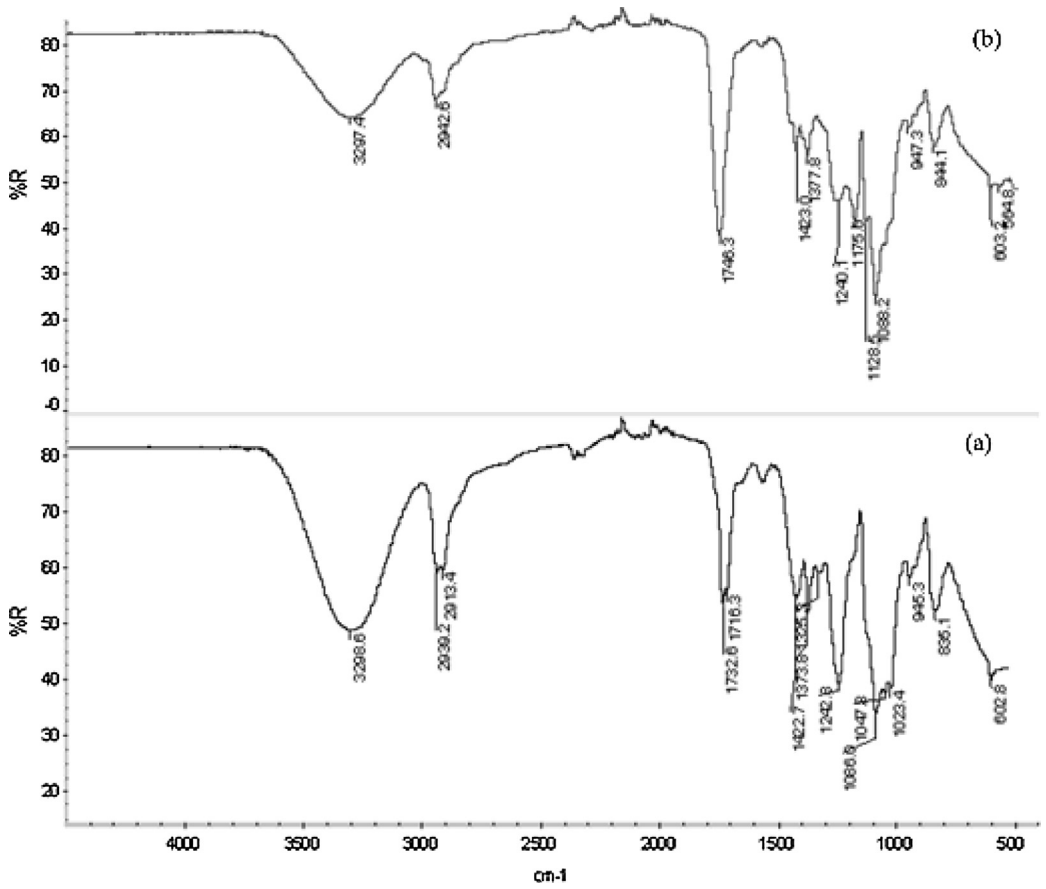

Fig. 5. FT-IR spectra of (a) NPs and (b) NPs-Fe_3O_4.

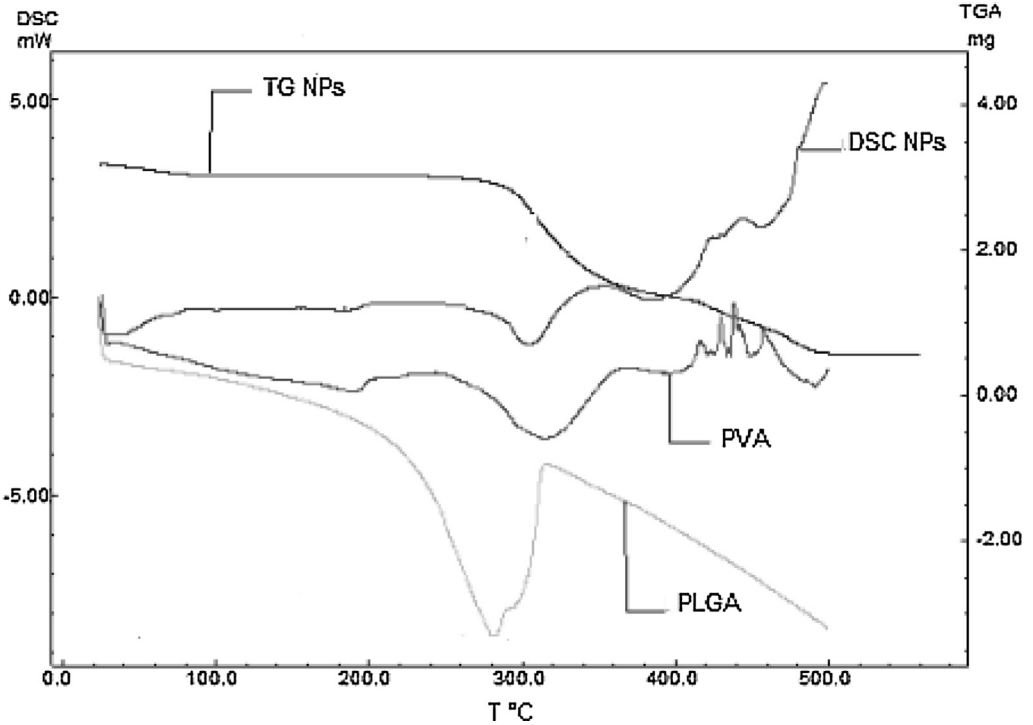

Fig. 6. DSC and TG thermograms of PVA, PLGA and NPs (50 nm).

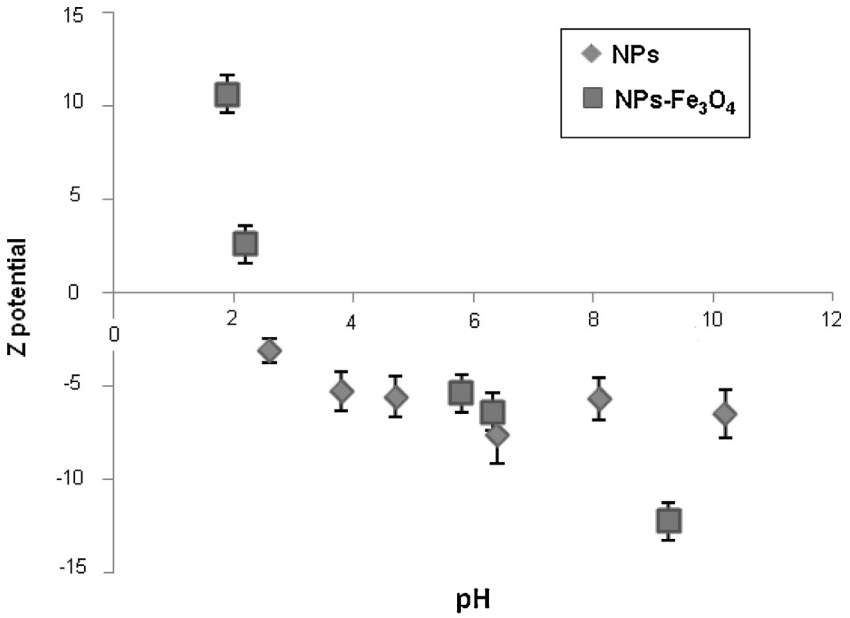

Fig. 7. *Z* potential of NPs (■) and NPs-Fe_3O_4 (◆) versus pH. Results represents the mean ± S.E. of three different experiments (1.49 for NPs and 2.44 for NPs-Fe_3O_4).

2.8.4. Quantum yield of singlet oxygen production

The quantum yield of singlet oxygen generation rates (Φ_Δ) was calculated by means of standard chemical monitor bleaching rates [29]. Imidazole (8 mM) and *N*,*N*-diethyl-4-nitrosoaniline (40–50 μM) in pH 7.4 phosphate buffer were used for all nanoparticles as a singlet oxygen chemical quencher [30]. The bleaching of nitrosoaniline was followed spectrophotometrically at 440 nm as a function of time. Polychromatic irradiation was performed using a projector lamp (Philips 7748SEHJ, 24V-250W), and a cut-off filter at 630 nm (Schott, RG 630) and a water filter were used to prevent infrared radiation. Both the nanoparticles and references (MB: $\Phi_\Delta = 0.56$ in phosphate buffer) [29] were irradiated within the same wavelength interval $\lambda_1 - \lambda_2$, and Φ_Δ was calculated according to Ref. [26].

3. Results and discussion

3.1. Characterization of nanoparticles

3.1.1. Particle size distribution and morphology

Figs. 2 and 3 show the size and morphology of NPs and NPs-Fe_3O_4 synthesized using four sonication cycles [31]. Fig. 4 shows that the size of the NPs depended on the number of the sonication cycles. Fig. 4 shows NPs size versus number of sonication cycles. The nanoparticles had an average size of 50 nm using four sonication cycles. The incorporation of magnetite into the NPs did not change their size.

3.1.2. Structural characterization

3.1.2.1. FT-IR spectroscopy. Fig. 5 shows the spectrum of NPs and NPs-Fe_3O_4. The FT-IR spectrum was collected over the range between 500 and 3500 cm^{-1}. A peak at 1746 cm^{-1} for the ester band of PLGA and at 3300–2900 cm^{-1} for the OH group of PVA was observed.

The characteristic peak for magnetite corresponding to Fe–O stretching was observed at 564.8 cm^{-1} [32].

3.1.2.2. Differential scanning calorimetry. Fig. 6 shows the DSC curves, which provided qualitative and quantitative information about the NPs components (PLGA, PVA, and PLGA–PVA). Pure PVA shows two endothermic peaks at 320 °C and 380 °C. These data were confirmed by the thermogram (TG) curve of pure PVA, which shows that the maximum weight loss (94.09%) occurred at 227.4 °C. Pure PLGA exhibited an endothermic event at 200 °C. The TG of pure PLGA shows that the polymer presented thermal stability up to 250 °C. The weight loss of pure PLGA, attributed to

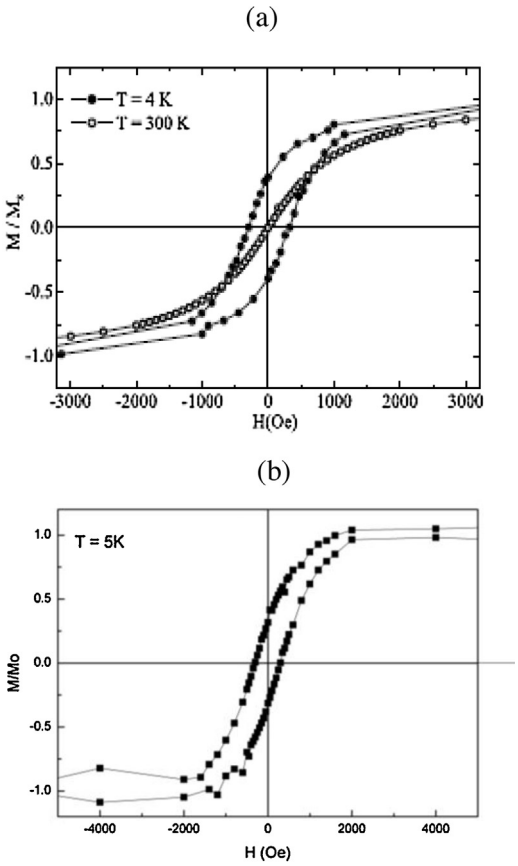

Fig. 8. Normalized hysteresis curves: (a) magnetite with PEI; (b) magnetite with PEI incorporated into NPs.

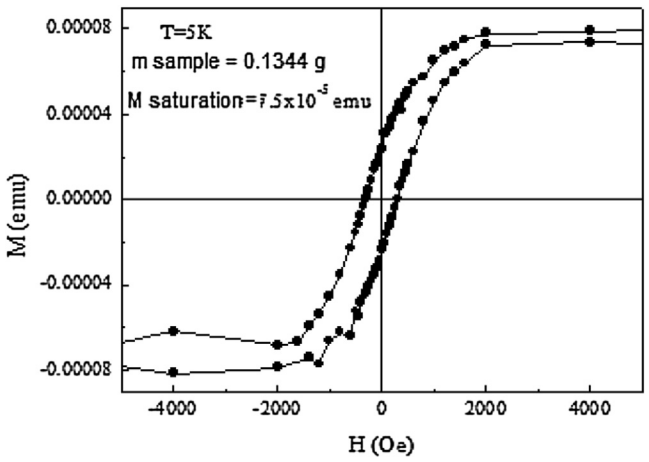

Fig. 9. Hysteresis curve of magnetite with PEI incorporated into NPs.

thermal decomposition, occurred at 181.8 °C—96.55%. The DSC curves of the physical mixture of PVA and PLGA showed peaks resulting from simple superposition of the DSC curves of the separate components. Thus, no interaction could be attributed to the heating process.

Overlapping of all the thermograms allowed observing that in the final NPs system, the peak corresponding to the decomposition of PVA appears first and that the one corresponding to the decomposition of PLGA appears next. This confirms that PVA is effectively stabilizing the polymer in the nanoparticle system (see Fig. 6).

3.1.2.3. Z potential of NPs and NPs-Fe_3O_4. The zeta potential values for NPs ranged from 10.21 to −12.26 mV [33]. The addition of magnetite to the system generated higher stabilization of the particles surface by means of negative potential values between −3.13 and −6.46 mV. These values were obtained in the total range of pH (Fig. 7).

3.1.2.4. Magnetic measurements and determination of magnetite incorporation into NPs. Fig. 8 shows the hysteresis loop of magnetite (a) and magnetite incorporated into NPs (b). Both curves show two clear different behaviors: at room temperature the superparamagnetic regime (reversible behavior) with zero coercive field, and the blocked regime with coercive field H_c = 300 Oe at T = 4 K. This behavior is an evidence of the low magnetic anisotropy of the superparamagnetic moment of the particles, probably due to the small nanoparticle size. At 5 K the same behavior was observed for NPs-Fe_3O_4 and for magnetite. The system retained its magnetic properties at T = 5 K with a blocked regime.

To calculate the magnetite incorporation into NPs we used the hysteresis loop of magnetite without normalization (Fig. 9). Samples were prepared in a ratio of 20% of magnetite [34]. According to the saturation values of the magnetization the degree of incorporation of magnetite was 0.3% [21].

The low percentage of incorporation of magnetite was due to several factors: (i) concentrations of 20 mg of magnetite per 100 mg of PLGA are accepted for clinical application [34]; (ii) PEI-stabilized magnetite is amphiphilic; thus, during the preparation it can be extracted by the aqueous phase containing PVA.

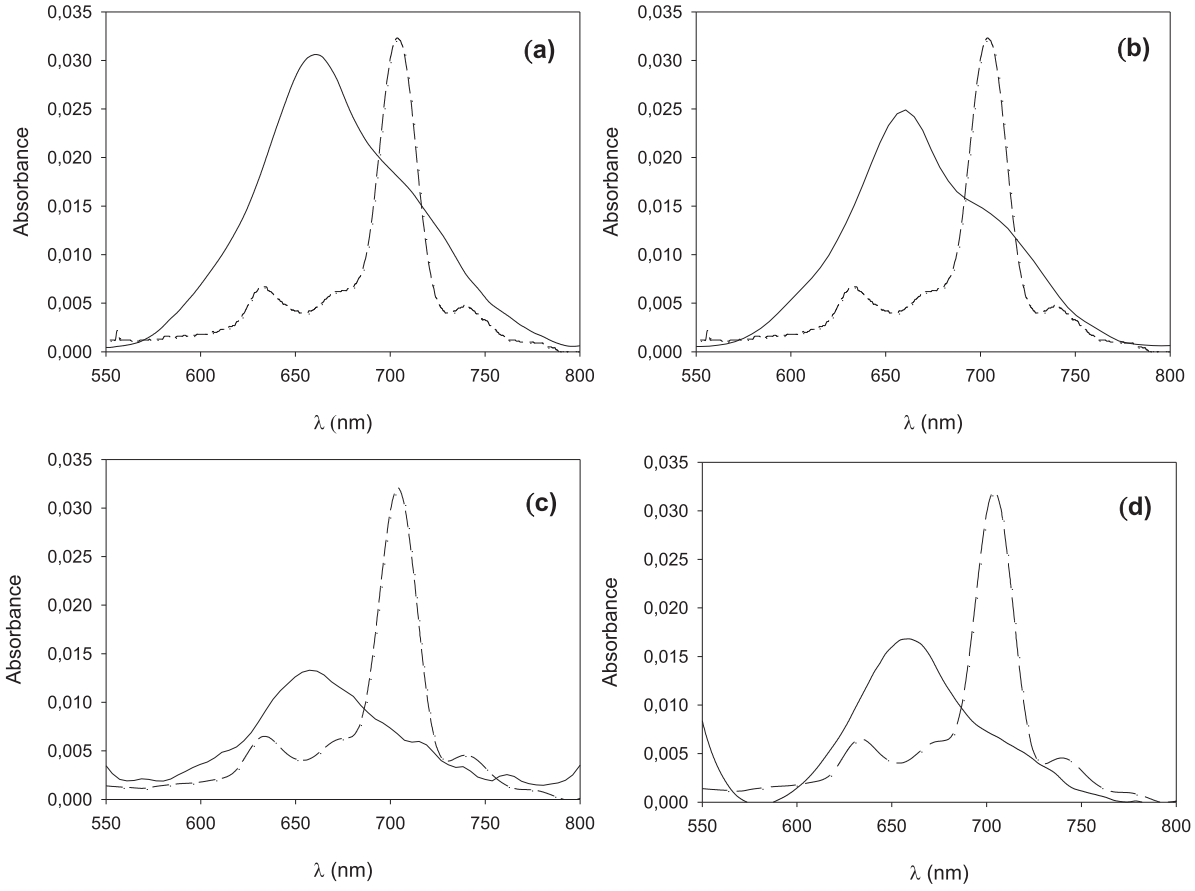

Fig. 10. Absorption spectra: (a) [S1] = 3.2 × 10^{-7} M in THF (—) and NPs (——). (b) [S1] = 3.2 × 10^{-7} M in THF (—) and NPs-Fe_3O_4 (——). (c) [S1] = 4.8 × 10^{-5} M in THF (—) and NPs (——). (d) [S1] = 4.8 × 10^{-5} M in THF (—) and NPs-Fe_3O_4 (——).

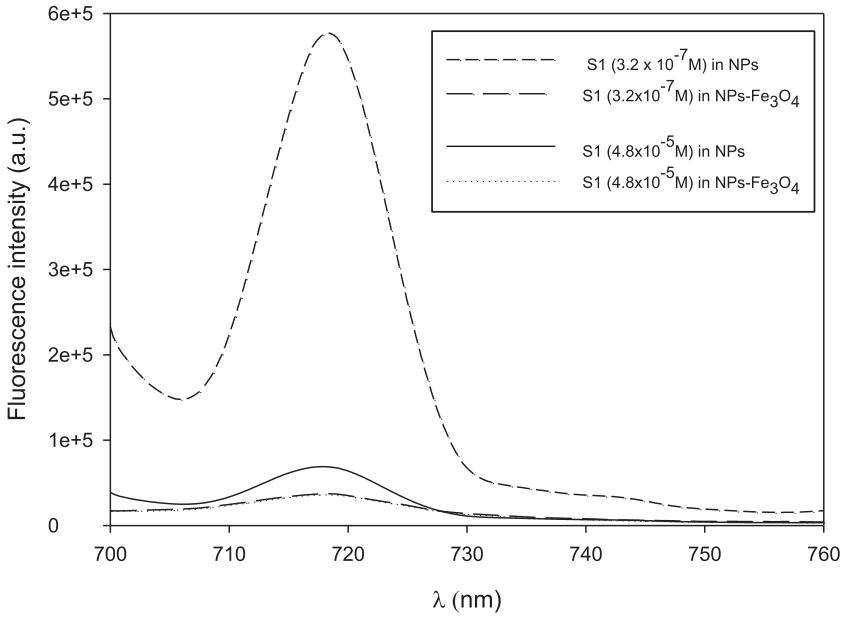

Fig. 11. Fluorescence spectra of NPs, S1-NPs, and S1-NPs-Fe_3O_4.

3.2. Photophysical properties

3.2.1. Spectroscopic studies

PLGA concentration in the suspensions was between 2×10^{-5} M and 6.7×10^{-6} M. The concentration of S1 in the nanoparticles was 3.2×10^{-7} M and 4.8×10^{-5} M. The absorption spectra of these nanoparticles were calculated according to Eq. (1) and compared with the spectrum of S1 in THF; at the concentration of 1×10^{-7} M where S1 is not aggregated (see Fig. 10).

The intensity absorption ratio of the two bands corresponding to the monomer and oligomers was calculated as described in Section 2.8.2 [35,36]. The analysis of the data in Table 1 shows that the inclusion of magnetite into the nanoparticles did not change the monomer/dimer ratio. In addition, increasing the dye concentration increased the aggregation in the nanoparticles.

3.2.2. Emission spectra and fluorescence quantum yields

Fig. 11 shows that the greatest emission intensity of S1-NPs corresponded to the lowest concentration of the dye due to its higher monomerization. On the other hand, NPs-Fe_3O_4 showed a similar value of intensity for both concentrations of S1 and lower than those of the S1-NPs systems. Similar values of fluorescence intensity were obtained for both concentrations of S1-NPs-Fe_3O_4. These values were lower than those obtained for S1-NPs. A similar behavior was observed for Φ_F values (Table 1).

3.2.3. Quantum yield of singlet oxygen production

Table 1 shows the Φ_Δ values of S1-NPs and S1-NPs-Fe_3O_4 at 3.2×10^{-7} M and 4.8×10^{-5} M. These values were calculated using MB in buffer and incorporated in NPs. No difference was observed using either system. For higher concentrations of S1 incorporated into NPs, smaller Φ_Δ values were obtained, due to the increase in S1 aggregation. The incorporation of magnetite into the nanoparticles, showed an increase in the values of Φ_Δ which is noteworthy at 4.8×10^{-5} M. At this concentration the effect of aggregation is lower than the effect of heavy atom or paramagnetic ions that deactivate the singlet excited state increasing the probability of intersystem crossing to the excited triplet state.

4. Conclusions

PLGA nanoparticles have advantages over other vehicles used for drug delivery. PLGA has been approved by the Food and Drug Administration (FDA) for 30 years for a variety of applications for human beings. The amount and rate of drug release can be controlled through mechanisms that are well known. A wide range of large and small as well as hydrophobic and hydrophilic molecules may be encapsulated into PLGA. The concentration of the stabilizer, and the number of cycles in the process of sonication during the synthesis of nanoparticles determine the size of the spheres, the value of the zeta potential, and the loading and release of the drug.

In the present study, it was shown that if a smaller particle size is desired, a greater number of sonication cycles should be used. The PVA stabilization of all the nanoparticles synthesized provided a negative charge to the systems over a wide pH range. The surface charge allows the suspension of the nanoparticles in a buffer solution at physiological pH, allowing its application for medical purposes. The thermograms obtained by DSC and TG show that the nanoparticles were stabilized by PVA, since the first peak corresponds to PVA.

The incorporation of magnetite nanoparticles was verified by FT-IR, magnetization measurements by means of hysteresis curves and *Z* potential. A photosensitizer (S1) incorporated in NPs and NPs-Fe_3O_4 was characterized, which retained S1 efficiency in generating singlet oxygen. The incorporation of magnetite into the nanoparticles showed an increase in the values of Φ_Δ, due to the heavy atom effect.

Acknowledgments

This work was supported by grants from the University of Buenos Aires, the Consejo Nacional de Investigaciones Científicas y Técnicas (CONICET), and the Agencia Nacional de Promoción Científica y Tecnológica, Argentina. We also wish to thank the language supervision by Mrs María Victoria Gonzalez Eusevi.

References

[1] N.C. López Zeballos, M.C. García Vior, J. Awruch, L.E. Dicelio, An exhaustive study of a novel sulfur-linked adamantane tetrasubstituted zinc(II) phthalocyanine incorporated into liposomes, J.. Photochem. Photobiol. A 235 (2012) 7–13.

[2] C.F. van Nostrum, Polymeric micelles to deliver photosensitizers for photodynamic therapy, Adv. Drug Deliv. Rev. 56 (2004) 9–16.

[3] M.C. García Vior, E. Monteagudo, L.E. Dicelio, J. Awruch, A comparative study of a novel lipophilic phthalocyanine incorporated into nanoemulsion formulations: photophysics, size, solubility and thermodynamic stability, Dyes Pigm. 91 (2011) 208–214.

[4] M. Gaspar Tosato, D.E. Orallo, M.S. Churio, A.A. Martín, C.A. Telléz Soto, L.E. Dicelio, Influence of mycosporine-like aminoacids and gadusol on the rheology and Raman spectroscopy of polymer geles, Biorheology 51 (2014) 315–328.

[5] N.C. Lopez Zeballos, M.C. García Vior, J. Awruch, L.E. Dicelio, A comparative study of peripheral and non-peripheral zinc (II) phthalocyanines incorporated into mesoporous silica nanoparticles, Dyes Pigm. 113 (2015) 145–150.

[6] M.C. Daniel, D. Astruc, Gold Nanoparticles: assembly, supramolecular chemistry, quantum-size-related properties, and applications toward biology, catalysis, and nanotechnology, Chem. Rev. 104 (2004) 293–346.

[7] F. Ye, A. Barrefelt, H. Asem, M. Abedi-Valugerdi, I. El-Serafi, M. Saghafian, K. Abu-Salah, S. Alrokayan, M. Muhammed, M. Hassan, Biodegradable polymeric vesicles containing magnetic nanoparticles, quantum dots and anticancer drugs for drug delivery and imaging, Biomaterials 35 (2014) 3885–3894.

[8] Y. Zhang, T. Chen, Targeting nanomaterials: future drugs for cancer chemotherapy, Int. J. Nanomed. 7 (2012) 5283–5286.

[9] A.-H. Lu, E.L. Salabas, F. Schüth, Magnetic nanoparticles: synthesis, protection, functionalization, and application, Angew. Chem. Int. Ed. 46 (2007) 1222–1244.

[10] F. Zhang, J. Jin, X. Zhong, S. Li, J. Niu, R. Li, J. Ma, Pd immobilized on amine-functionalized magnetite nanoparticles: a novel and highly active catalyst for hydrogenation and Heck reactions, Green Chem. 13 (2011) 1238–1243.

[11] E. Ranjbakhsh, A.K. Bordbar, M. Abbasi, A.R. Khosropour, E. Shams, Enhancement of stability and catalytic activity of immobilized lipase on silica-coated modified magnetite nanoparticles, Chem. Eng. J. 179 (2012) 272–276.

[12] D.E. Sosnovik, M. Nahrendorf, R. Weissleder, Magnetic nanoparticles for MR imaging: agents, techniques and cardiovascular applications, Basic Res. Cardiol. 103 (2008) 122–130.

[13] D.B. Shenoy, M.M. Amiji, Poly (ethylene oxide)-modified poly-(caproloctone) nanoparticles for target delivery of tamoxifen in breast cancer, Int. J. Pharm. 293 (2005) 261–270.

[14] Y.N. Konan, M. Berton, R. Gurny, E. Allemann, Enhanced photodynamic activity of meso-tetra(4-hydroxyphenyl) porphyrin by incorporation into sub-200 nm nanoparticles, Eur. J. Pharm. Sci. 18 (2003) 241–249.

[15] E. Ricci-Junior, J.M. Marchetti, Zinc(II) phthalocyanine loaded PLGA nanoparticles for photodynamic therapy use, Int. J. Pharm. 310 (2006) 187–195.

[16] S. Essa, J.M. Rabanel, P. Hildgen, Effect of polyethylene glycol (PEG) chain organization on the physicochemical properties of poly(D, L-lactide) (PLA) based nanoparticles, Eur. J. Pharm. Biopharm. 75 (2010) 96–106.

[17] D. Chen, Q. Tang, X. Li, X. Zhou, J. Zang, W. Xue, J. Xiang, C. Guo, Biocompatibility of magnetic Fe_3O_4 nanoparticles and their cytotoxic effect on MCF-7 cells, Int. J. Nanomed. 7 (2012) 4973–4982.

[18] M. Mahmoudi, S. Sant, B. Wang, S. Laurent, T. Sen, Superparamagnetic iron oxide nanoparticles (SPIONs): development, surface modification and applications in chemotherapy, Adv. Drug Deliv. Rev. 63 (2011) 24–46.

[19] Wahajuddin S. Arora, Superparamagnetic iron oxide nanoparticles: magnetic nanoplatforms as drug carriers, Int. J. Nanomed. 7 (2012) 3445–3471.

[20] V.E. Diz, G.A. Gauna, C.A. Strassert, J. Awruch, L.E. Dicelio, Photophysical properties of microencapsulated phthalocyanines, J. Porphyrins Phthalocyanines 14 (2010) 278–283.

[21] J.M. Vargas, R.D. Zysler, Tayloring the size in colloidal iron oxide magnetic nanoparticles, Nanotechnology 16 (2005) 1474–1476.

[22] S. Gürsoy, A. Cihan, M.B. Kocak, Ö. Bekaroglu, Synthesis of new metal-free and metal-containing phthalocyanines with tertiary or quaternary aminoethyl substituents, Monatsh. Chem. 132 (2001) 813–819.

[23] C. Pinto Reis, R.J. Neufeld, A.J. Ribeiro, F. Veiga, Nanoencapsulation II. Biomedical applications and current status of peptide and protein nanoparticulate delivery systems, Nanomedicine 2 (2006) 53–65.

[24] Y. Cu, W.M. Saltzman, Controlled surface modification with poly(ethylene) glycol enhances diffusion of PLGA nanoparticles in human cervical mucus molecules, Pharmaceutics 6 (2008) 173–181.

[25] M.G. Lagorio, Reflectance spectroscopy using wine bottle glass, J. Chem. Educ. 76 (1999) 1551–1554.

[26] S. Amore, M.G. Lagorio, L.E. Dicelio, E. San Roman, Photophysical properties of supported dyes. Quantum yield calculations in scattering media, Prog. React. Kinet. Mech. 26 (2001) 159–177.

[27] M.E. Rodriguez, F. Morán, A. Bonansea, M. Monetti, D.A. Fernández, C.A. Strassert, V. Rivarola, J. Awruch, L.E. Dicelio, A comparative study of photophysical and phototoxic properties of a new octaalkyl zinc (II) phthalocyanine incorporated in an hydrophilic polymer, in liposomes and in non ionic micelles, Photochem. Photobiol. Sci. 2 (2003) 988–994.

[28] E. Alarcón, A.M. Edwards, A.M. Garcia Muñoz, A. Aspée, C.D. Borsarelli, E.A. Lissi, Photophysics and photochemistry of zinc phthalocyanine/bovine serum albumin adducts, Photochem. Photobiol. Sci. 8 (2009) 255–263.

[29] F. Wilkinson, W.P. Herman, A.D. Rose, Rate constant for the decay and reactions of the lowest electronically excited singlet state of molecular oxygen in solution. An expanded and revised compilation, J. Phys. Chem. Ref. Data 24 (1995) 663–1021.

[30] I. Kraljic, S. El Mohsni, A new method for the detection of singlet oxygen in aqueous solutions, Photochem. Photobiol. 28 (1978) 577–581.

[31] J. Vandervoort, K. Yoncheva, A. Ludwig, Influence of the homogenisation procedure on the physicochemical properties of PLGA nanoparticles, Chem. Pharm. Bull. 52 (2004) 1273–1279.

[32] A.G. Roca, Preparación de nanopartículas nanomagnéticas uniformes y de alta cristalinidad para biomedicina, Tesis Doctoral, Departamento de Química Física, Instituto de Ciencia de Materiales de Madrid, CSIC, Universidad Complutense de Madrid, España, 2009.

[33] C. Barrera, A. Herrera, Y. Zayas, C. Rinaldi, Surface modification of magnetite nanoparticles for biomedical applications, J. Magn. Magn. Mater. 321 (2009) 1397–1399.

[34] R. Hergt, A.W. Andra, C.G. d'Ambly, I. Hilger, W.A. Kaiser, U. Richter, H.G. Schmidt, Physical limits of hyperthermia using magnetite fine particles, IEEE Trans. Magn. 34 (1998) 374–375.

[35] C.A. Strassert, G.M. Bilmes, J. Awruch, L.E. Dicelio, Comparative photophysical investigation of oxygen and sulfur as covalent linkers on octaalkylamino substituted zinc(II) phthalocyanines, Photochem. Photobiol. Sci. 7 (2008) 738–747.

[36] M.E. Rodríguez, D.A. Fernández, J. Awruch, S. Braslavsky, L.E. Dicelio, Effect of aggregation of a cationic phthalocyanine in micelles and in the presence of human serum albumin, J. Porphyrins Phthalocyanines 10 (2006) 33–42.